

Supplementary Information

Controlling the Photoluminescence Chromaticity of Emissive Copper Nanoclusters

via Ligand Engineering

Mengfan Chang^{+[a]}, Ying Xu^{+[a]}, Ying Lv^a, Haizhu Yu^a, Hao Li^{*[b]}, Xi Kang^{*[a]}, Manzhou Zhu^[a]

[a] Department of Chemistry and Centre for Atomic Engineering of Advanced Materials, Key Laboratory of Structure and Functional Regulation of Hybrid Materials of Ministry of Education, Anhui Province Key Laboratory of Chemistry for Inorganic/Organic Hybrid Functionalized Materials, Anhui University, Hefei, Anhui 230601, P. R. China.

[b] School of Materials and Chemical Engineering, Anhui Jianzhu University, Hefei, Anhui 230601, P. R. China.

[+] These authors contributed equally to this work.

E-mails of corresponding authors: kangxi_chem@ahu.edu.cn (X.K.); haoli96@ahjzu.edu.cn (H.L.)

This Supporting Information file includes:

Experimental Methods

Figures S1-S17

Tables S1-S3

Experimental Methods

Chemical Materials

All reagents are purchased from Sigma-Aldrich and used directly without further purification: cupric acetate monohydrate $[(\text{CH}_3\text{COO})_2\text{Cu}\cdot\text{H}_2\text{O}]$, 99.0%, metal basis], copper(I) chloride, *p*-methylbenzenethiolate ($\text{C}_7\text{H}_7\text{S}$, *p*-MBT, 98%), *p*-(tert-butyl)benzenethiol (TBBT, $\text{C}_{10}\text{H}_{14}\text{S}$), *m*-aminobenzenethiol ($\text{C}_6\text{H}_7\text{NS}$, *m*-ABT), triphenylphosphine ($\text{C}_{18}\text{H}_{15}\text{P}$, PPh_3 , 99%), tris(4-fluorophenyl)phosphine ($\text{C}_{18}\text{H}_{12}\text{F}_3\text{P}$, $\text{P}(\text{Ph}^f\text{F})_3$, 99%), sodium borohydride (NaBH_4 , 99%), dichloromethane (CH_2Cl_2 , HPLC grade), methanol (CH_3OH , HPLC grade), *n*-hexane (C_6H_{14} , HPLC grade), and acetonitrile (CH_3CN , HPLC grade).

Synthesis of the $\text{Cu}_8(\textit{p}\text{-MBT})_8(\text{PPh}_3)_4$ nanocluster

For the synthesis of the $\text{Cu}_8(\textit{p}\text{-MBT})_8(\text{PPh}_3)_4$ nanocluster, please refer to the method reported by Li et al. ^[1] The absolute yield was 24.85mg and the percentage yield was calculated to be 38.84% based on the Cu element for the **Cu8a** nanocluster.

Synthesis of the $\text{Cu}_8(\text{TBBT})_8(\text{PPh}_3)_4$ nanocluster

For the synthesis of the $\text{Cu}_8(\text{TBBT})_8(\text{PPh}_3)_4$ nanocluster, 40 mg of copper acetate (dissolved in 10 mL of CH_3OH) and 50 mg of PPh_3 were added to 15 mL of dichloromethane in a 50 mL round bottom flask with vigorously stirred (~ 1200 rpm). After 60 minutes, 67 μL of TBBT was added and the solution turned to light yellow. After 4 hours, 8 mL of methanol was added to the reaction, and the mixed solution was evaporated at room temperature. Then, yellow crystals of the $\text{Cu}_8(\text{TBBT})_8(\text{PPh}_3)_4$ nanocluster were obtained. The absolute yield was 25.03mg and percentage yield was calculated to be 34.56% based on the Cu element for the **Cu8b** nanocluster.

Synthesis of the $\text{Cu}_8(\textit{m}\text{-ABT})_8[\text{P}(\text{Ph}^f\text{F})_3]_4$ nanocluster

For the synthesis of the $\text{Cu}_8(\textit{m}\text{-ABT})_8[\text{P}(\text{Ph}^f\text{F})_3]_4$ nanocluster, 50 mg of cuprous chloride (dissolved in 4 mL of CH_3CN) and 50 μL of *m*-ABT were added to 15 mL of dichloromethane in a 50 mL round bottom flask with vigorously stirred (~ 1200 rpm). After 60 minutes, 120 mg of $\text{P}(\text{Ph}^f\text{F})_3$ was added to the above solution. After another 40 minutes, 60 mg of NaBH_4 (dissolved in 1 mL of H_2O) was quickly added to the solution. The reaction was proceeded for 12 hours. After the solvent evaporation, the crude product was dissolved in 20 mL of CH_2Cl_2 and centrifuged at 10000 rpm for 1 minute to remove the precipitate. Then, the crude product was washed by hexane to get the pure cluster product. The crystals of the $\text{Cu}_8(\textit{m}\text{-ABT})_8[\text{P}(\text{Ph}^f\text{F})_3]_4$ nanocluster were obtained by liquid diffusing the *n*-hexane into the dichloromethane solution of the nanocluster for three days. The absolute yield was 83.90mg and the percentage yield was calculated to be 47.83% based on the Cu element for the **Cu8c** nanocluster (60.49% based on the S element).

Single-crystal X-ray diffraction

The data collection for single-crystal X-ray diffraction of three Cu_8 nanoclusters was carried out on a Stoe Stadivari diffractometer under nitrogen flow using graphite-monochromatized Cu $\text{K}\alpha$ radiation ($\lambda = 1.54186\text{\AA}$). Using Olex2, the structure was solved with the ShelXT structure solution program using Intrinsic Phasing and refined with the ShelXL refinement package using least-squares minimization. All the non-hydrogen atoms were found directly. All the non-hydrogen atoms were refined anisotropically. All the hydrogen atoms were set in geometrically calculated

positions and refined isotropically using a riding model. The diffuse electron densities resulting from the residual solvent molecules were removed from the data set using the SQUEEZE routine of PLATON and refined further using the data generated.

Characterization

UV-vis absorption spectra in the solution state were collected on a PerkinElmer Lambda 465 spectrophotometer. UV-vis absorption spectra in the solid state were carried on a Shimadzu 3600-plus spectrophotometer with an integrating sphere.

PL spectra, absolute PL quantum yield (PLQY) and emission lifetimes were measured on a HORIBA FluoroMax-4P.

The PL lifetime was fitted by the DAS6 Analysis software. The PL lifetime of the **Cu8a** and **Cu8c** crystal was calculated by a third-order exponential fitting. The PL lifetime of **Cu8b** crystals was fitted by a second-order exponential fitting.

Electrospray ionization mass (ESI-MS) was performed on Waters XEVO G2-XSQT of mass spectrometer. The samples are dissolved in a mixture solution of CH₂Cl₂/CH₃OH (v:v = 1:1), which is directly infused into the chamber at 10 μL min⁻¹ with positive mode.

X-ray photoelectron spectroscopy (XPS) measurements were performed on an ESCALAB 250Xi XPS spectrometer. The XPS of three kinds of Cu₈ nanoclusters were fitted by Avantage.

The CCDC numbers of Cu₈(*m*-ABT)₈[P(Ph^{*p*}F)₃]₄ is 2422705.

Computational Details.

The modeled Cu₈(SPh)₈(PPh₃)₄ was calculated at the PBE/DND level^[2] with the effective core potential pseudopotential^[3-4] performed in the DMol3 package.^[5-7] The convergence tolerances of energy, force, and displacement for the structure relaxation were 1.0 × 10⁻⁶ Ha, 2.0 × 10⁻⁴ Ha/Å, and 5.0 × 10⁻⁴ Å, respectively. Based on the calculated structures, the calculation of UV-vis spectrum was carried out at the time-dependent PBE/DND level^[2], and the lowest 100 singlet-singlet excited states were calculated.

References

- [1] Li, H. Wang, T. Han, J. Xu, Y. Kang, X. Li, X. et al. Nat. Commun. 2024, 15, 5351.
- [2] Perdew, J. P.; Burke, K.; Ernzerhof, M. Phys. Rev. Lett. 1996, 77, 3865.
- [3] Dolg, M.; Wedig, U.; Stoll, H.; Preuss, H. J. Chem. Phys. 1987, 86, 866.
- [4] Bergner, A.; Dolg, M.; Kuechle, W.; Stoll, H.; Preuss, H. Mol. Phys. 1993, 80, 1431.
- [5] Delley, B. J. Chem. Phys. 1990, 92, 508.
- [6] Delley, B. J. Chem. Phys. 1996, 100, 6107.
- [7] Delley, B. J. Chem. Phys. 2000, 113, 7756.

Acknowledgements

The numerical calculations in this paper have been done on Hefei advanced computing center.

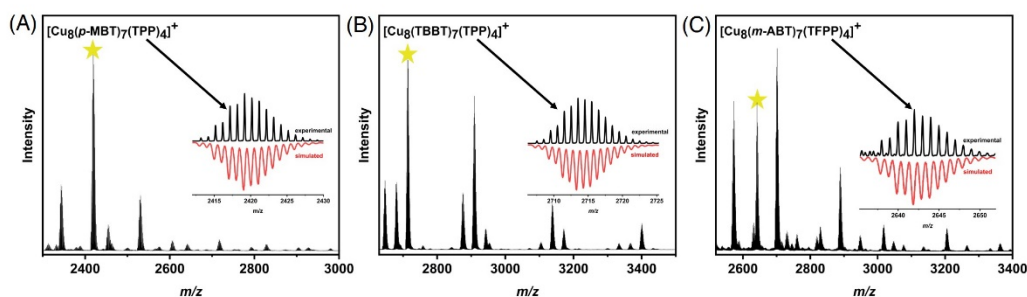


Figure S1. ESI-MS results of (A) **Cu8a**, (B) **Cu8b**, and (C) **Cu8c** nanoclusters in the positive mode. Insets: the experimental and simulated isotope patterns.

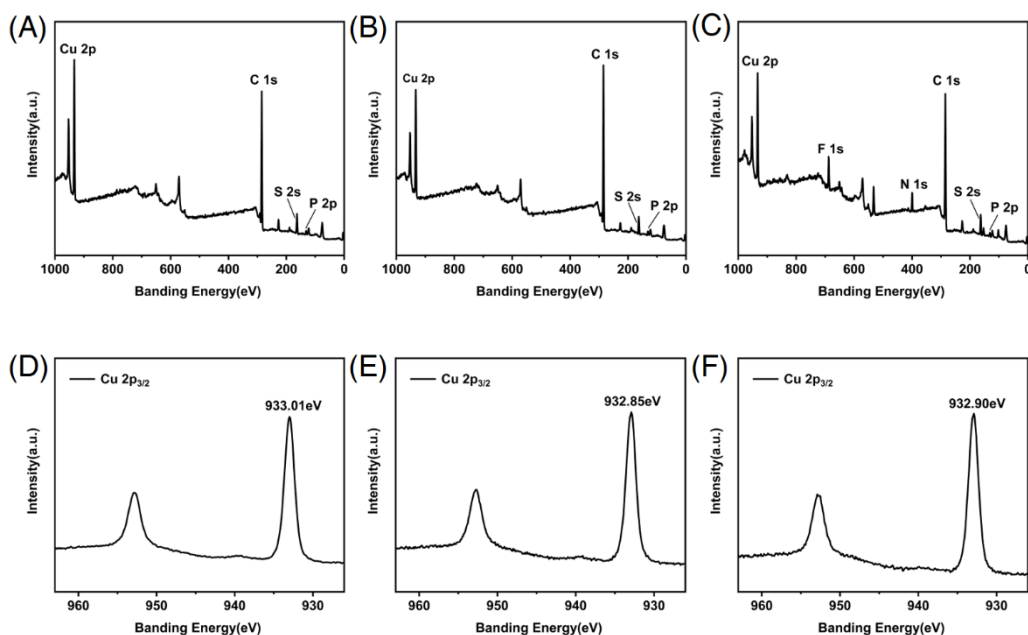


Figure S2. (A) XPS result of **Cu8a**. (B) XPS result of **Cu8b**. (C) XPS result of **Cu8c**. (D) XPS results of the Cu 2p bands in **Cu8a**. (E) XPS results of the Cu 2p bands in **Cu8b**. (F) XPS results of the Cu 2p bands in **Cu8c**.

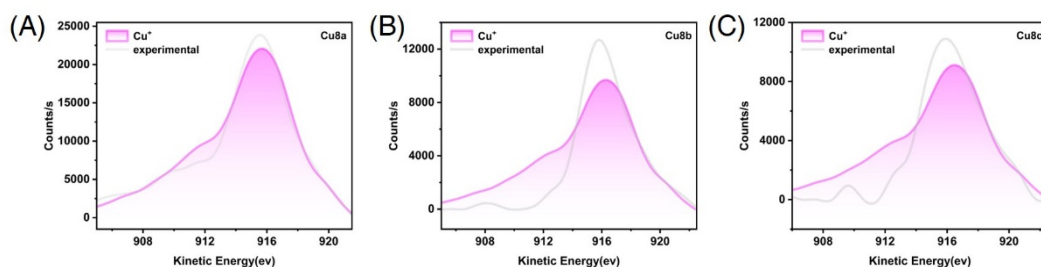


Figure S3. Cu LMM results of **Cu8a**, **Cu8b**, and **Cu8c** nanoclusters. (A) Cu LMM X-ray-excited Auger electron spectroscopy of **Cu8a**. (B) Cu LMM X-ray-excited Auger electron spectroscopy of **Cu8b**. (C) Cu LMM X-ray-excited Auger electron spectroscopy of **Cu8c**.

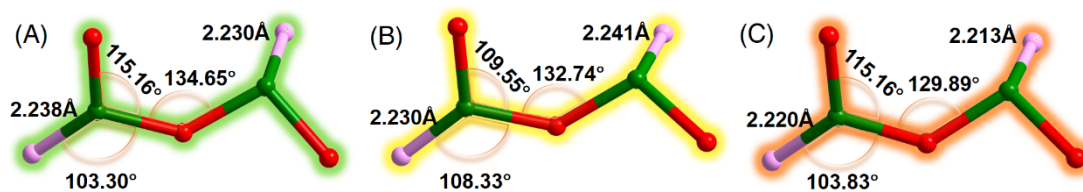


Figure S4. Detailed comparison of bond distances of Cu-P and corresponding angles in the $\text{Cu}_2\text{S}_3\text{P}_2$ motif of (A) **Cu8a**, (B) **Cu8b**, and (C) **Cu8c** nanoclusters.

As mentioned in the manuscript, the ligand effect influenced the superlattice crystalline packing modes of metal nanoclusters. Specifically, both **Cu8a** and **Cu8c** cluster molecules were crystallized in the triclinic system P-1, while the crystalline packing system of **Cu8b** was the monoclinic I2/a (Figures S5-7).

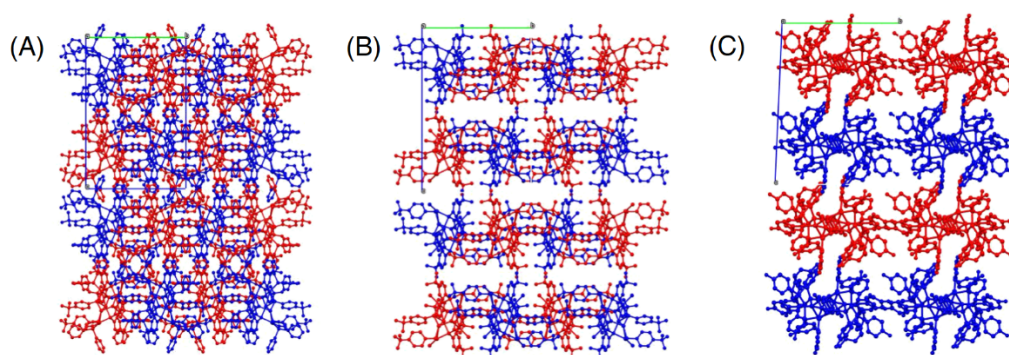


Figure S5. Crystalline assembled packing modes of (A) **Cu8a**, (B) **Cu8b**, and (C) **Cu8c** cluster molecules viewed along a axis.

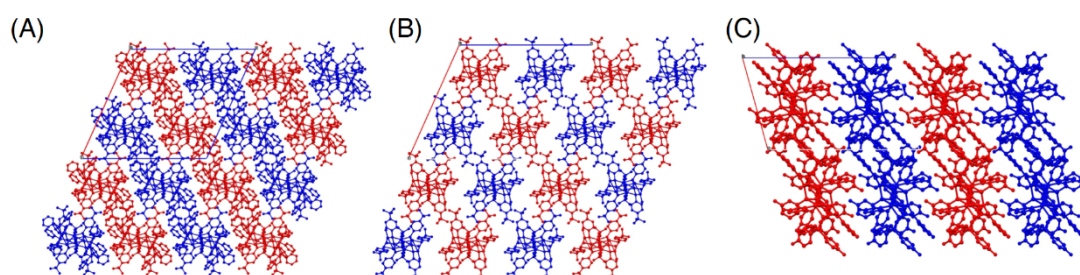


Figure S6. Crystalline assembled packing modes of (A) **Cu8a**, (B) **Cu8b**, and (C) **Cu8c** cluster molecules viewed along b axis.

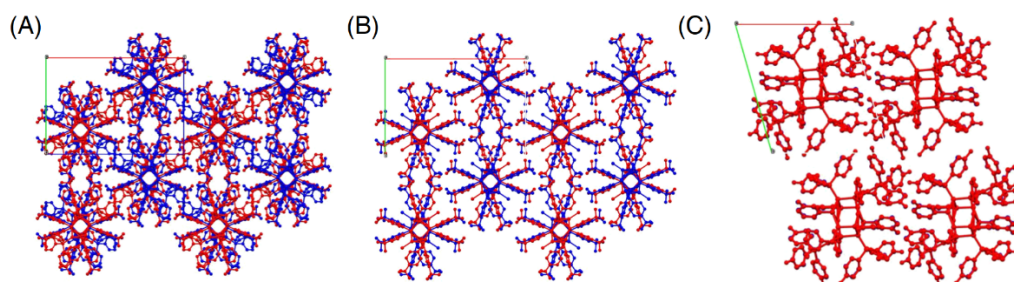


Figure S7. Crystalline assembled packing modes of (A) **Cu8a**, (B) **Cu8b**, and (C) **Cu8c** cluster molecules viewed along *c* axis.

The different superlattice crystalline packing modes of these three Cu₈ nanoclusters resulted from their distinct interactions. For instance, in **Cu8a**, several C-H \cdots π and H \cdots H intermolecular interactions were observed between two adjacent cluster molecules (Figure S8A), while only H \cdots H intermolecular interactions were detected between **Cu8b** cluster molecules (Figure S8B). By comparison, the **Cu8c** nanoclusters not only displayed C-H \cdots π and H \cdots H interactions between ligands but also featured several N \cdots H and F \cdots H interactions (Figure S8C). In addition, the supramolecular arrangement of metal nanoclusters in their crystal lattice was also supported by their weak interaction strength. By comparison, it is evident that **Cu8a** exhibits a stronger C-H \cdots π and $\pi\cdots\pi$ interaction (Figures S9-S11).

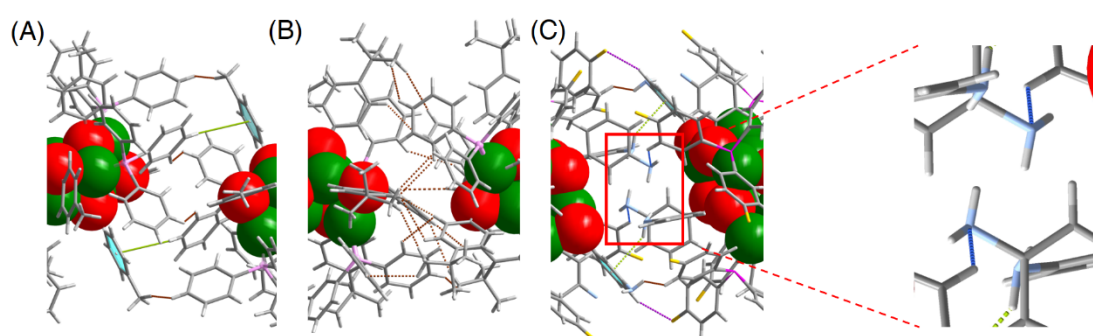


Figure S8. Intercluster interactions in the crystalline unit cells of **Cu8a**, **Cu8b**, and **Cu8c** nanoclusters. (A) C-H \cdots π and H \cdots H interactions in **Cu8a** cluster. (B) H \cdots H interactions between ligands in **Cu8b** cluster. (C) C-H \cdots π , N \cdots H, F \cdots H, and H \cdots H interactions between ligands in **Cu8c** cluster. Specifically, C-H \cdots π interactions were marked in green, N \cdots H interactions were marked in blue, F \cdots H interactions were marked in purple, and H \cdots H interactions were marked in brown. Color labels: green, Cu; red, S; gray, C; pink or purple, P; blue, N; yellow, F.

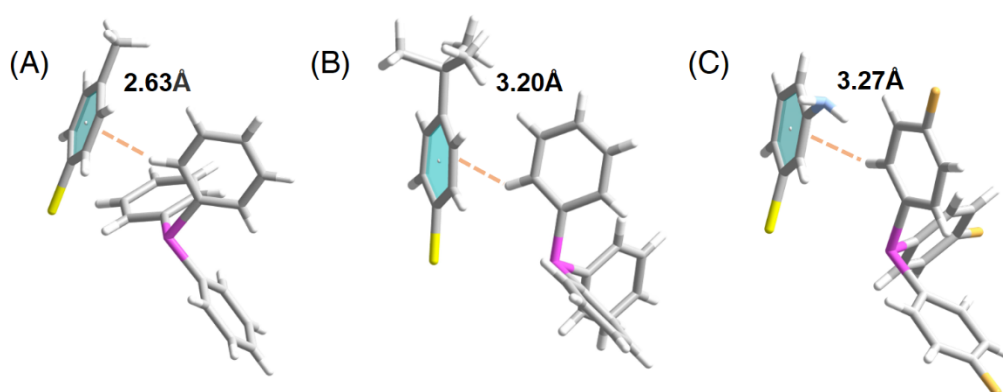


Figure S9. C-H \cdots π interactions on the surface of (A) **Cu8a**, (B) **Cu8b**, and (C) **Cu8c** nanoclusters.

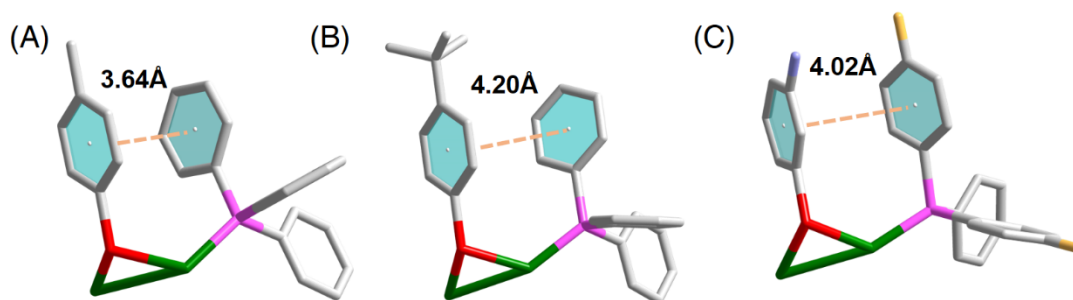


Figure S10. $\pi\cdots\pi$ interactions on the surface of (A) **Cu8a**, (B) **Cu8b**, and (C) **Cu8c** nanoclusters.

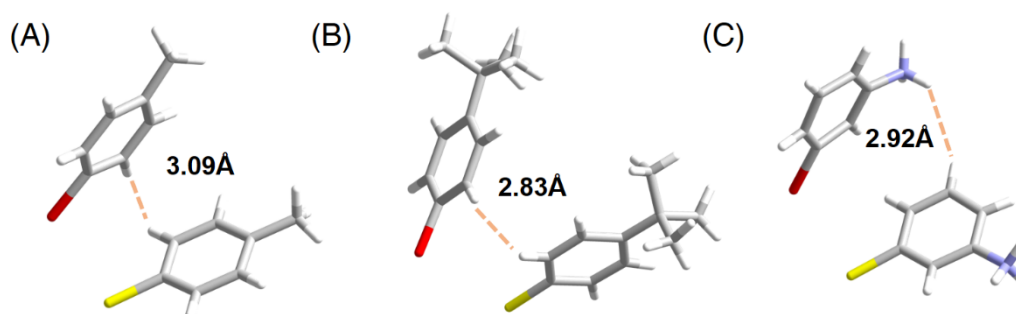


Figure S11. $H\cdots H$ interactions on the surface of (A) **Cu8a**, (B) **Cu8b**, and (C) **Cu8c** nanoclusters.

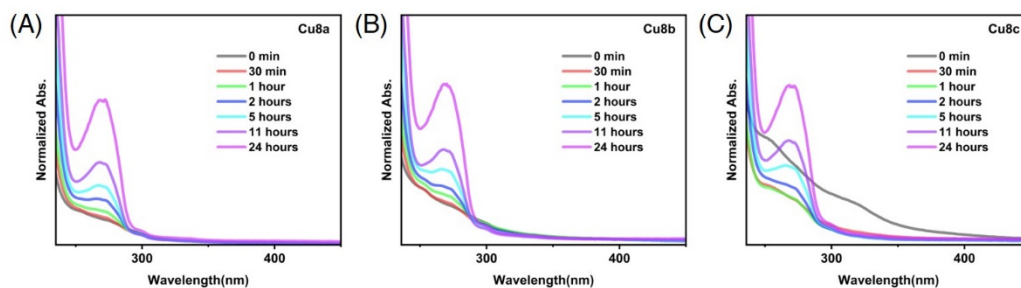


Figure S12. The time-dependent UV-Vis spectra of the (A) **Cu8a**, (B) **Cu8b**, and (C) **Cu8c** nanoclusters in CH_2Cl_2 solvent.

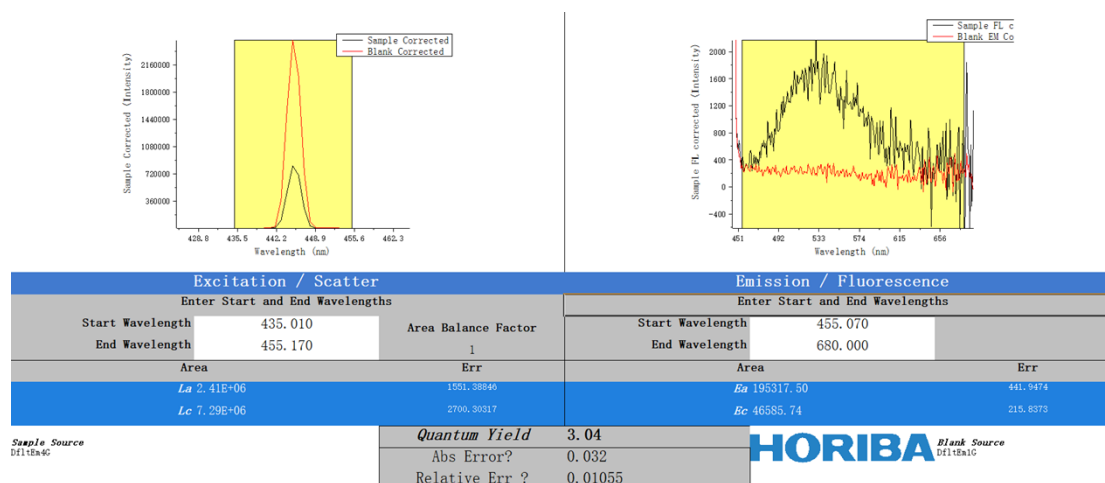


Figure S13. The absolute PLQY at room temperature of the **Cu8a** nanocluster (crystalline states).

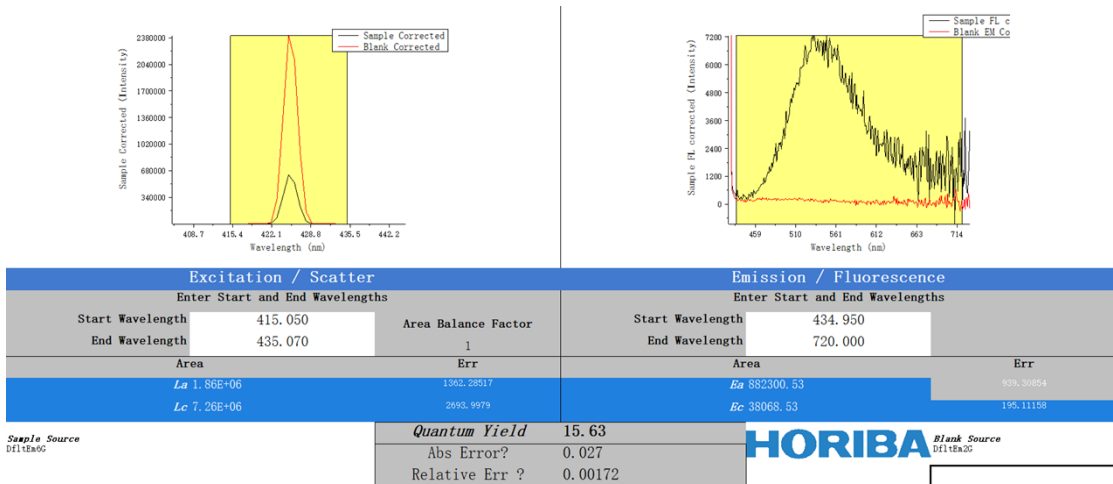


Figure S14. The absolute PLQY at room temperature of the **Cu8b** nanocluster (crystalline states).

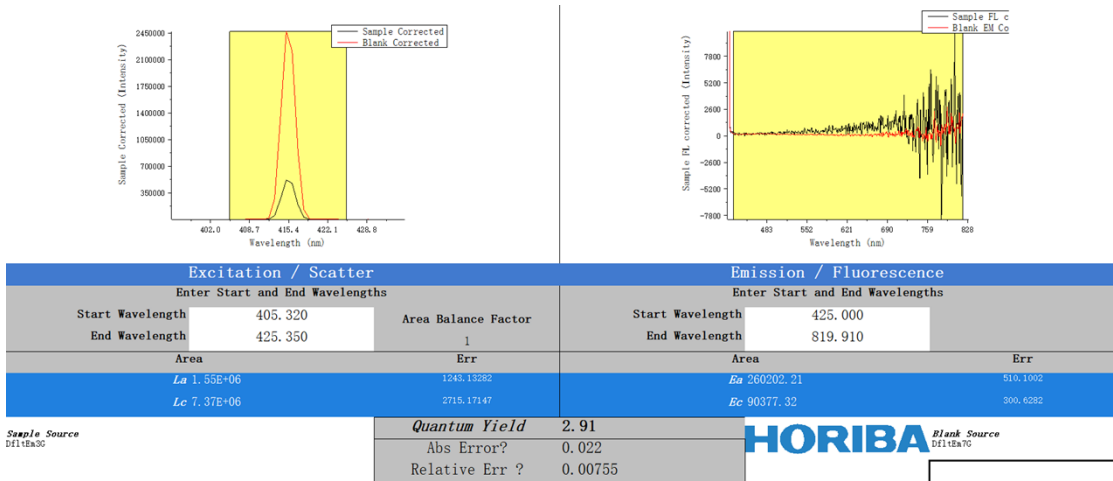


Figure S15 The absolute PLQY at room temperature of the **Cu8c** nanocluster (crystalline states).

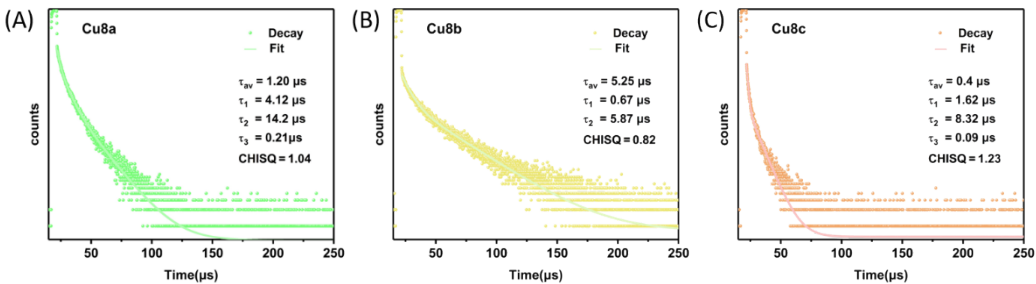


Figure S16. The PL lifetime of (A) **Cu8a**, (B) **Cu8b**, and (C) **Cu8c** nanoclusters at room temperature.

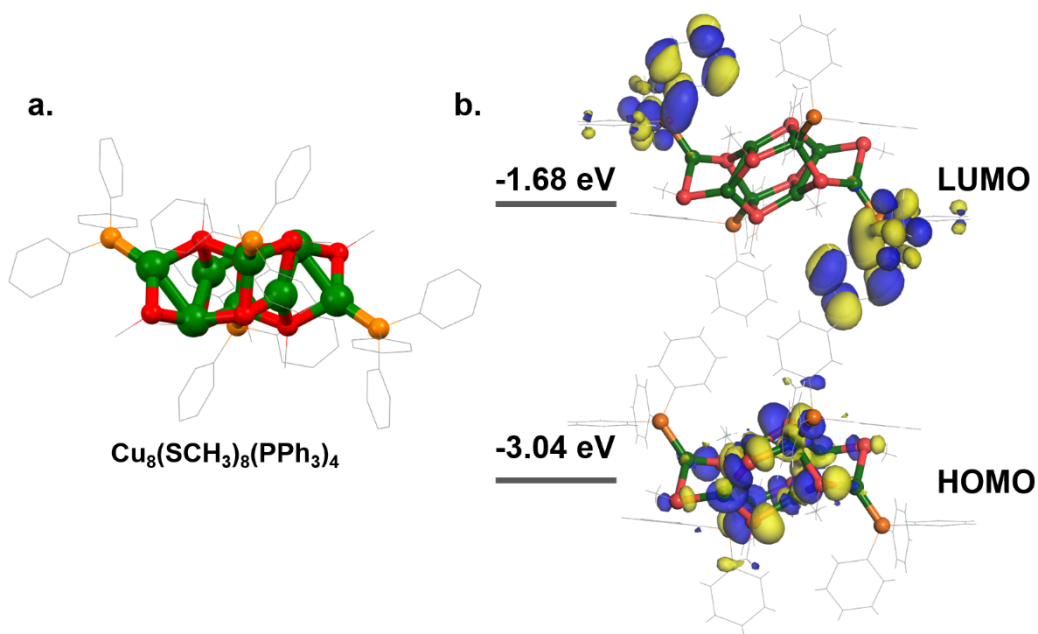


Figure S17. (A) The modeled $\text{Cu}_8(\text{SCH}_3)_8(\text{PPh}_3)_4$ cluster. (B) The electron densities of HOMO and LUMO in $\text{Cu}_8(\text{SCH}_3)_8(\text{PPh}_3)_4$.

Theoretical calculations identified that a HOMO-LUMO energy gap of 1.36 eV for the optimized structure (Figure S17B), and the Highest Occupied Molecular Orbital (HOMO) primarily arises from the Cu-S framework, whereas the Lowest Unoccupied Molecular Orbital (LUMO) predominantly distributed on triphenylphosphine ligands.

Table S1. Detail comparison of bond distances of Cu-Cu, Cu-S, and Cu-P in three Cu_8 nanoclusters

Cluster	Cu-Cu distance range Å (average Å)	Cu-S distance range Å (average Å)	Cu-P distance range Å (average Å)
Cu8a	2.759-2.882(2.821)	2.222-2.410(2.312)	2.230-2.238(2.234)
Cu8b	2.812-2.873(2.851)	2.218-2.436(2.305)	2.230-2.241(2.236)
Cu8c	2.726-3.075(2.877)	2.206-2.258(2.304)	2.207-2.250(2.298)

Table S2. The parameters of multi-exponential fits for luminescence decay of **Cu8a**, **Cu8b** and **Cu8c** NCs.

Cluster	Cu8a	Cu8b	Cu8c
$\tau_1(\mu\text{s})$	4.12	0.67	1.62
$\tau_2(\mu\text{s})$	14.20	5.87	8.32
$\tau_3(\mu\text{s})$	0.21	/	0.09
$B_1(\%)$	40.09	1.52	39.85
$B_2(\%)$	45.14	98.48	40.48
$B_3(\%)$	14.77	/	19.67
$\tau_{\text{av}}(\mu\text{s})$	1.20	5.25	0.40
CHISQ	1.04	0.82	1.23

Table S3. Crystal data and structure refinement for the **Cu8c** nanocluster.

Empirical	$C_{121}H_{98}Cl_2Cu_8F_{12}N_8P_4S_8$
Formula weight	2851.65
Temperature (K)	120
Crystal system	triclinic
Space group	P-1
a (Å)	12.2639(6)
b (Å)	16.0411(8)
c (Å)	17.8781(9)
α (°)	74.241(4)
β (°)	88.232(4)
γ (°)	74.805(4)
Volume (Å ³)	3263.5(3)
Z	1
ρ_{calc} (g cm ³)	1.451
μ (mm ⁻¹)	3.978
F(000)	1442.0
Crystal size (mm ³)	0.24 × 0.16 × 0.09
Radiation	Cu K α (λ = 1.54186)
2 θ range for data collection (°)	9.26 to 141.678
Index ranges	-14 ≤ h ≤ 10, -16 ≤ k ≤ 19, -19 ≤ l ≤ 21
Reflections collected	24287
Independent reflections	11855 [R_{int} = 0.0650, R_{sigma} = 0.0599]
Data/restraints/parameters	11855/0/749
Goodness-of-fit on F^2	1.033
Final R indexes [$I \geq 2\sigma(I)$]	R_1 = 0.0794, wR_2 = 0.2218
Final R indexes [all data]	R_1 = 0.1010, wR_2 = 0.2495
Largest diff. peak/hole (e Å ⁻³)	1.25/-0.63